Stepwise magnetization reversal of geometrically tuned in diameter Ni and FeCo bi-segmented nanowire arrays

Ester M. Palmero[1,3] (✉), Miguel Méndez[2], Silvia González[2], Cristina Bran[1], Víctor Vega[2], Manuel Vázquez[1], and Víctor M. Prida[2]

[1] *Institute of Materials Science of Madrid (ICMM-CSIC), Madrid 28049, Spain*
[2] *Department of Physics, University of Oviedo, Federico García Lorca 18, Oviedo 33007, Spain*
[3] *Division of Permanent Magnets and Applications, IMDEA Nanoscience, Madrid 28049, Spain*

ABSTRACT

Magnetization reversal processes of hexagonal dense arrays of bi-segmented Ni and $Fe_{50}Co_{50}$ nanowires consisting of two well defined diameters (45 and 80 nm) have been studied. The nanowires were grown inside of tailored pores of anodic alumina templates by combined anodization, atomic layer deposition (ALD) and electrodeposition techniques. The experiments have allowed to identify their two-step magnetization reversal process ascribed to the respective segments of different diameter. This is concluded from the differential susceptibility observed in the hysteresis loops, contrary to those for nanowires with homogeneous diameter. These results are also confirmed by the first-order reversal curve (FORC) distribution diagrams, where an elongation parallel to the interaction axis around two coercive field values is obtained, which is correlated to the difference in diameter of the two segments. This well-defined two-step magnetization reversal process through the nanowire diameter design is thought to be very useful for the advanced control of the remagnetization in arrays of magnetic multidomain systems.

KEYWORDS

Bi-segmented nanowires, nickel, iron cobalt alloy, stepwise magnetization reversal, first-order reversal curve (FORC)

1 Introduction

Nowadays, the modulation in diameter imprinted along the length of magnetic nanowires has become as a promising route to tailor their magnetic properties, allowing for a controlled motion of magnetic domain walls (DWs) and the possibility to manipulate the DW displacement by applying magnetic fields for their implementation in new-generation devices for information storage, logic system and sensors [1–8]. Cylindrical nanowires with modulated diameter and specific compositions are fabricated by different techniques such as the combination of mild and hard anodization processes [9–11] or by anodization together with atomic layer deposition (ALD) technique [12–17]. The magnetization reversal process of the nanowires can be severely modified by the modulation in diameter, as the modulation might serve as pinning centers for controlling the domain wall movement from one nanowire end to the other [10, 18–20]. In this sense, for the development of high-tech information storage devices, ferromagnetic nanowires with modulated diameter, and more specific having well defined and abrupt difference in nanowires segment diameter, offer the possibility of controlling the domain wall movement along the nanowire and thus making more difficult its displacement in the opposite direction.

The magnetic behavior of a nanowire array is determined by the intrinsic magnetization of individual nanowires (i.e. competition between magnetocrystalline and shape anisotropies), and also by the magnetostatic interactions among neighboring nanowires. Nanowires with polycrystalline crystallographic structure (e.g. Ni nanowires with face-centered cubic (fcc) or FeCo nanowires with body-centered

cubic (bcc) crystalline phases) show reduced magnetocrystalline anisotropy [21–23]. For these nanowire arrays, the magnetization reversal processes are highly influenced by the shape anisotropy and, consequently by any modification of the nanowire geometry (e.g. diameter modulation) and segmentation [18, 19, 24, 25]. It was shown that the magnetization reversal in nanowires takes place by the domain wall nucleation at the ends of the nanowire, depinning and its subsequent propagation along the nanowire length [26–29].

Hysteresis loops measurements are commonly used for studying the magnetic properties of nanowire arrays. However, to understand the magnetic behavior of each nanowire having a particular tuned geometry and composition, together with their magnetic interactions into the array, a more specific analysis must be performed. In this sense, first-order reversal curve (FORC) technique is a proven powerful method for the analysis of the magnetization reversal processes and magnetostatic interactions and the quantification of their effects on the final magnetic properties in many-body interacting systems, such as nanowire, nanopillar or nanotube arrays, antidots and multilayer films [20, 30–36].

In the literature only a few studies can be found about cylindrical bi-segmented nanowires [14, 16, 17] and they are mainly focused on soft magnetic materials (e.g. permalloy, FeNi or CoNi) for the synthesis of bi-segmented nanowires with narrow and wide segments ranging between 120 and 450 nm. In this work we report on the intrinsic magnetic behavior of magnetically soft (Ni) and hard (FeCo) bi-segmented diameter modulated nanowire arrays with reduced wide and narrow nanowire diameters (in the range of 30–80 nm) fabricated by a combined method of anodization,

ALD and electrodeposition techniques. Magnetic measurements by vibrating sample magnetometry (VSM), together with the analysis through FORC method of the magnetostatic interactions among the nanowires inside the array have been correlated with a detailed geometrical and crystallographic study of the nanowires by high resolution transmission electron microscopy (HRTEM). These geometrically engineered in diameter bi-segmented ferromagnetic nanowires can be employed as novel magnetic multidomain systems for ultrahigh-density data storage applications.

2 Experimental

2.1 Synthesis of bi-segmented nanowires

Nanoporous alumina membranes with hexagonally ordered pores modulated in diameter were prepared by a combined process consisting on mild anodization, pore widening and ALD steps on 99.999% Al foil substrates. The two-step anodization was performed by using oxalic acid aqueous solution, after the preparation of a smooth Al surface, leading to a highly hexagonally ordered nanopores arrangement (Fig. 1(a)). The diameter of this first segment was slightly enlarged by chemical pore widening to obtain the first segment of the alumina nanopores, which will host the segment with smaller diameter of the geometrically modulated nanowires. Afterwards, ALD technique was used to grow a protective layer of SiO_2 to avoid the further chemical etching of this narrow segment (Fig. 1 (b)) [37]. Subsequently, a further anodization step was performed under the same conditions as the first and second ones but for longer time. The nanoporous alumina membranes were then immersed in phosphoric acid aqueous solution to enlarge the pore diameter of the second wider segment, whereas the smaller diameter section of the first alumina nanopore segment coated with the protective SiO_2 layer deposited by ALD remained unchanged (Fig. 1(c)). After that, the remaining Al at the backside and the alumina barrier layer were chemically etched, and an additional ALD process was performed to swell a protective surface layer of SiO_2 for covering the whole nanowires. Patterned alumina membranes with nanopores of uniform diameter along their length (without geometrical modulations) were also grown for comparison. More information about the parameters used in anodization, pore widening and ALD processes can be found in the Electronic Supplementary Material (ESM).

In order to fabricate a working electrode for nanowires electro-deposition, a gold layer was deposited by sputtering and electroplating

Figure 1 Scheme of the samples fabrication procedure. (a) Highly ordered nanoporous alumina template obtained by two-step mild anodization. (b) SiO_2 ALD surface functionalization. (c) Third anodization and selective pore widening steps. (d) SiO_2 ALD surface functionalization of the diameter modulated nanoporous alumina template and gold working electrode deposition. (e) Electrodeposition of bi-segmented magnetic nanowires array with modulated diameter. (f) SiO_2 coated, free-standing bi-segmented nanowires after being released from the alumina template by selective chemical etching.

on the narrow pores side of the alumina membranes to completely cover the pores (Fig. 1(d)). Afterwards, Ni and FeCo nanowires were grown into both, uniform and modulated diameter nanopores of the alumina membranes by electrodeposition (Fig. 1(e)). The composition of the electrolytic baths and the electrodeposition voltage are collected in Table S1 in the ESM.

2.2 Bi-segmented nanowires characterization

Scanning electron microscope (SEM) was used to estimate the geometrical parameters of the nanowire arrays: distance between nanowire centers and average nanowire diameters. HRTEM measurements were used to precisely determine the geometrical parameters, the diameter of each nanowire segment at the modulation of freestanding single nanowires, as well as the thickness of the protective SiO_2 layer, after releasing them from the alumina templates (Fig. 1(f)).

The chemical composition of the nanowires was determined by using an energy dispersive X-ray spectrometer (EDS) and their crystallographic structure was determined by X-ray diffractometer (XRD). A more detailed study of the crystallographic microstructure of the nanowires was carried out by the combination of HRTEM and selected area electron diffraction (SAED) measurements.

Hysteresis loops of bi-segmented diameter modulated and homogeneous diameter Ni and FeCo nanowire arrays were measured by VSM under magnetic fields applied parallel and perpendicular to the nanowire axis. FORC technique was employed to analyze the intrinsic magnetic behavior of the nanowire segments and study the magnetostatic interactions among the nanowires in the arrays. For each sample, the FORC distribution (ρ_{FORC}) was calculated and represented graphically by a contour plot indicating the statistical distribution of the mathematical hysterons in the sample. The coercive field, H_c, represents the width of the hysteresis loop for each hysteron, while the interaction field, H_u, denotes the shift of the hysteron along the field axis, being the non-interacting case represented by a symmetric hysteron [38]. More information about the protocol and parameters used for the FORC measurements can be found in the ESM.

3 Results and discussion

3.1 Nanowires geometry, composition and crystallographic structure

The geometrical parameters of the nanowires that have been considered for this study are: diameter (D_{NW1}, D_{NW2}) and length (L_1, L_2) of the narrow and wide segments (Fig. 2(a)); nanowire diameter (D) and total length (L) for nanowires with homogeneous diameter; distance between nanowire centers in the array (D_{int} = 105 nm for all the nanowire arrays); and the thickness of the SiO_2 protective layer for bi-segmented nanowires was th_1 = 9 nm and th_2 = 4 nm, for the narrow and wide segments, respectively. The geometrical features of the bi-segmented diameter modulated nanowire are depicted in the scheme of Fig. 2(a) and the corresponding values of the geometrical parameters for the samples studied here are collected in Tables 1 and 2 for both, bi-segmented and straight nanowire arrays, respectively. The sharpness and high uniformity of the diameter modulation in the bi-segmented nanopores of the alumina template can be observed in the SEM image of Fig. 2(b). The morphology of this geometrical modulation is then reproduced by the nanowires, which were grown by electrochemical deposition inside the tailored pores of the alumina template, as evidenced in Fig. 2(c).

The morphology and microstructure of two sets of samples (nanowires arrays with bi-segmented and homogeneous diameter) that were fabricated with different magnetic materials, Ni and FeCo alloy, were checked by XRD analysis. From the XRD spectra (Fig. S1
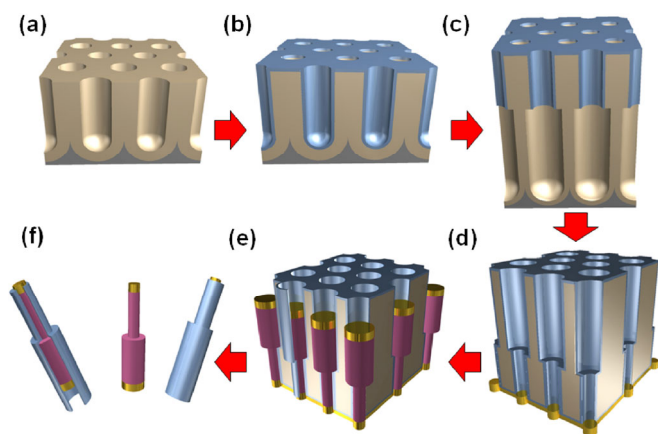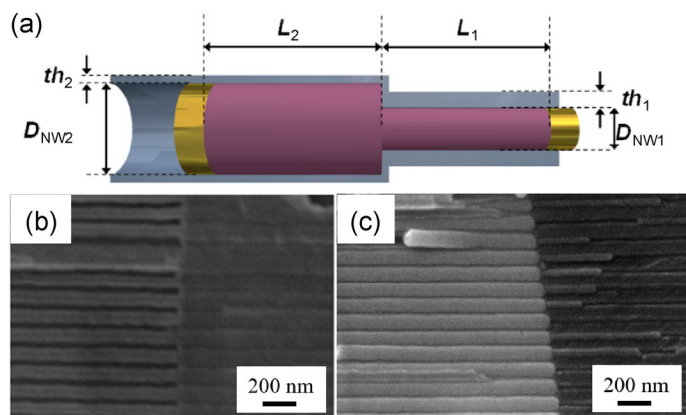
Figure 2 (a) Scheme of the bi-segmented nanowire geometry, including the geometrical parameters considered in the study, where D_{NW1} and D_{NW2}, L_1 and L_2, are the diameters and their respective lengths of the narrow and thicker segments of the bi-segmented nanowire, while th_1 and th_2 refer to the SiO_2 layer thickness covering each segment, respectively. SEM cross section images of (b) a nanoporous alumina template with bi-segmented nanopores, and (c) a bi-segmented FeCo nanowire array, where the bright region at the left of the image indicates higher density of magnetic material (wide segments), while the dark region at the right side of the image shows the narrow segments.

Table 1 Composition and geometrical parameters (diameter and length of the narrow, D_{NW1} and L_1, and wide, D_{NW2} and L_2, segments) of bi-segmented nanowires

Sample	Composition	D_{NW1} (nm)	D_{NW2} (nm)	L_1 (μm)	L_2 (μm)
Ni-1	Ni	30	80	5.0 ± 1.0	5.0 ± 1.0
Ni-2	Ni	45	80	5.0 ± 1.0	7.0 ± 1.0
FeCo-1	$Fe_{50}Co_{50}$	30	80	3.3 ± 0.5	3.0 ± 0.5
FeCo-2	$Fe_{50}Co_{50}$	45	80	3.8 ± 0.5	2.8 ± 0.5
FeCo-3	$Fe_{50}Co_{50}$	45	80	3.3 ± 0.5	1.6 ± 0.5

Table 2 Composition and geometrical parameters (diameter, D, and length, L) of nanowires with homogeneous diameter

Sample	Composition	D (nm)	L (μm)
Ni-3	Ni	30	6.0 ± 1.0
Ni-4	Ni	45	5.0 ± 1.0
Ni-5	Ni	80	5.0 ± 1.0
FeCo-4	$Fe_{50}Co_{50}$	30	2.0 ± 1.0
FeCo-5	$Fe_{50}Co_{50}$	45	2.0 ± 1.0
FeCo-6	$Fe_{50}Co_{50}$	80	1.3 ± 1.0
FeCo-7	$Fe_{50}Co_{50}$	80	2.5 ± 1.0

in the ESM) it was determined that Ni nanowires crystallize in a polycrystalline fcc structure with (220) preferential growing direction and also showing (111) and (200) peaks. On the other hand, XRD patterns for FeCo nanowires show a polycrystalline bcc structure with (110) preferential growing direction.

Figure 3 shows the bright field HRTEM images and the SAED pattern of representative bi-segmented Ni and FeCo nanowires, respectively. The HRTEM image in Fig. 3(a) corresponds to a bi-segmented Ni nanowire from the sample Ni-1, which exhibits a sharp modulation in the diameter between the narrow and wide nanowire segments. Moreover, it can also be seen the protective SiO_2 layer that covers all the nanowire, as it is also confirmed in the EDS elemental mapping from Fig. 3(e). The SAED patterns were obtained both in the wide and narrow segments of the nanowire (Figs. 3(b) and 3(c), respectively). They exhibit a polycrystalline structure for the Ni nanowire, as demonstrated by the existence of diffraction rings indexed as (111), (200) and (220) sets of reflections
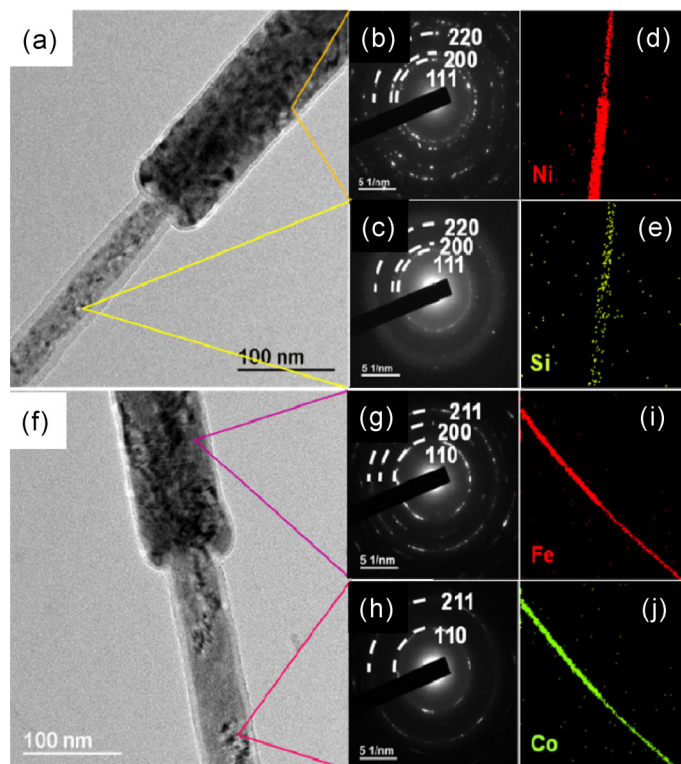

Figure 3 (a) HRTEM image of a bi-segmented Ni nanowire taken at the geometrical modulation from sample Ni-1. SAED patterns corresponding to the (b) wide and (c) narrow segments of the nanowire shown in (a). EDS mapping displaying the homogeneous distribution of (d) Ni and (e) Si on the cover of nanowire. (f) The HRTEM image of a bi-segmented FeCo nanowire corresponding to FeCo-2 sample. SAED patterns of the (g) wide and (h) narrow segments of the same nanowire shown in (a). EDS mapping exhibiting the homogeneous distribution of (i) Fe and (j) Co elements.

corresponding to a fcc structure, also observed in the XRD pattern obtained for the whole Ni nanowires array. The SAED images do not evidence great difference between the crystallographic structures of each segment of the bi-segmented Ni nanowires. Figures 3(d) and 3(e) display the chemical analysis performed by the EDS elemental mapping of the Ni nanowire to check its homogeneity along the nanowire length, and the presence of the SiO_2 layer covering the whole nanowire to prevent it from corrosion and oxidation.

Figure 3(f) displays a representative bright field HRTEM image of a bi-segmented FeCo nanowire corresponding to the FeCo-2 sample, which shows the geometrical modulation in the diameter and its protective silicon oxide layer. The SAED patterns of the wide and narrow segments of the FeCo nanowire displayed in Fig. 3(f) are shown in Figs. 3(g) and 3(h), respectively. The patterns present a polycrystalline bcc structure as demonstrated by the existence of diffraction rings indexed as (110), (200) and (211). The (200) and (211) reflections were not observed in the XRD patterns as they are not the preferential growing direction and also due to the signal background arising from the large amount of amorphous alumina of the template in which the nanowires are embedded, which impede their detection. However, in the SAED-HRTEM analysis, it is possible to detect these reflections as the nanowires are released from the alumina template. The main difference between the SAED patterns of both segments is that in the case of the narrow segment, the reflection corresponding to the (200) direction has disappeared, which can be ascribed to the reduction in diameter, therefore decreasing drastically the signal.

EDS analysis was performed on FeCo-2 nanowires sample to check the homogeneity of the alloy along the nanowire length. Figures 3(i) and 3(j) show the EDS chemical mapping obtained for a FeCo nanowire for both elements, Fe and Co, respectively. These

images show that both elements are homogeneously distributed along the nanowire, allowing us to state that the composition of the nanowire does not change significantly along the nanowire length.

3.2 Magnetic behaviour of bi-segmented nanowires

Figure 4 shows representative hysteresis loops obtained for both, Ni and FeCo diameter modulated bi-segmented and straight nanowire arrays, when the magnetic field is applied parallel and perpendicular to the nanowires axis, together with the anisotropy field distribution (AFD) curve, which has been calculated from the perpendicular hysteresis loops as AFD = $-H\, d^2M(H)/dH^2$, according to Refs. [39, 40]. Table S2 in the ESM summarizes the main magnetic parameters (coercive field, H_c, reduced remanence, M_r/M_s, and anisotropy field, H_A) obtained from hysteresis loops and AFD curves in Fig. 4.

For all the samples, the comparison between the hysteresis loops measured in both directions indicates that the easy magnetization axis lies parallel to the nanowire length, as evidenced by the higher values of coercivity and remanence of the parallel hysteresis loops compared to perpendicular ones. Moreover, the hysteresis loops of the bi-segmented nanowires present different values of the magnetic susceptibility along the range of the applied field (see Figs. 4(a) and 4(c)), being the first indication of a stepwise magnetization reversal process. This fact is more clearly evidenced in the appearance of two peaks in the AFD curves that can be observed for the bi-segmented nanowires. In the case of FeCo-1 sample (Fig. 4(c)), the two peaks are well separated and show maximum values of the AFD distribution at 5.11 and 10.04 kOe, which can be ascribed to H_A associated to the wide and narrow segments, respectively. However, in the case of bi-segmented Ni nanowires (Ni-2, Fig. 4(a)), the AFD peaks partially overlap, due to their larger width and the narrower difference in H_A values (at 2.23 and 4.34 kOe, respectively).

FORC distribution for each of the nanowire arrays was obtained by following the procedure described in the ESM. For all the FORC distributions, the values of coercive field (H_c^{FORC}) and interaction field (ΔH_u) have been obtained for Ni and FeCo nanowires and collected in Tables 3 and 4, respectively. The values for the two types of FORC distributions observed have been determined according to Refs. [31, 35]. In the FORC curves of the bi-segmented Ni nanowires (see minor hysteresis loops covering the hysteretic area in the insets of Figs. 5(a) and 5(b)), the existence of two regions with two different values of the magnetic susceptibility is even more evidenced, which is ascribed to magnetization reversal by steps. This type of magnetization reversal process is observed for
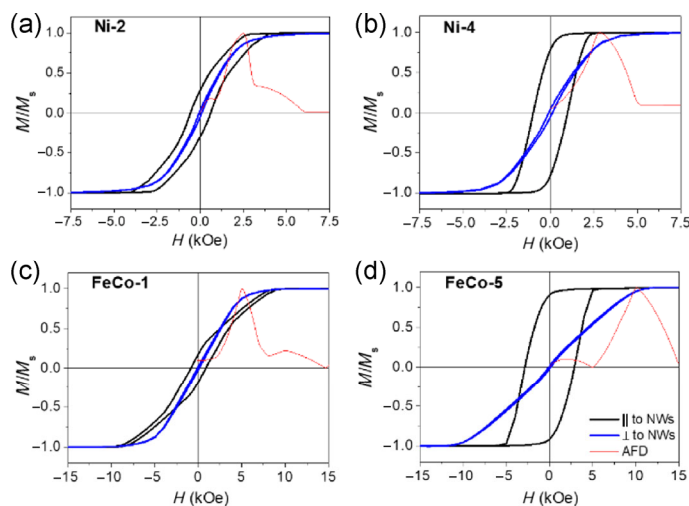
nanowires with geometrically modulated diameter when they are synthesized with an adequate ratio of the diameter modulation between the different segments, which is able to alter the domain wall motion [18, 24].

The measured FORC distributions for all the nanowire arrays represent systems where the magnetostatic interactions are demagnetizing, i.e. the interaction field is opposite to the magnetization [41]. In the FORC diagrams obtained for bi-segmented Ni nanowires (Figs. 5(a) and 5(b)), one can see that they present the general FORC distribution shape associated to a magnetic nanowire array with predominant shape anisotropy [33, 35, 42–45]. In this case, the FORC diagram is characterized by a single branch, which spreads widely parallel to the interaction field axis. The remarkable difference between these diagrams and the typical ones for nanowire arrays without diameter modulations is that this branch splits in two branches at two different values of coercive field (see the highlighting red ellipses in Figs. 5(a) and 5(b)). This fact is due to the difference in diameter of the two segments in the nanowires, which originates a different value of coercive field for each segment, as it has been well reported in the literature for nanowires with different diameter [23, 27]. For comparison, FORC diagrams for nanowires with homogeneous diameter were also obtained (Figs. 5(c) and 5(d)). In this case, only one branch parallel to the interaction field axis is observed. The size of the branch is larger for the FORC distribution in Fig. 5(d), which corresponds to the diagram for the array with straight nanowires and the larger value of nanowire diameter. In this case, the demagnetizing interactions (Table 3) increase due to the closer proximity of the
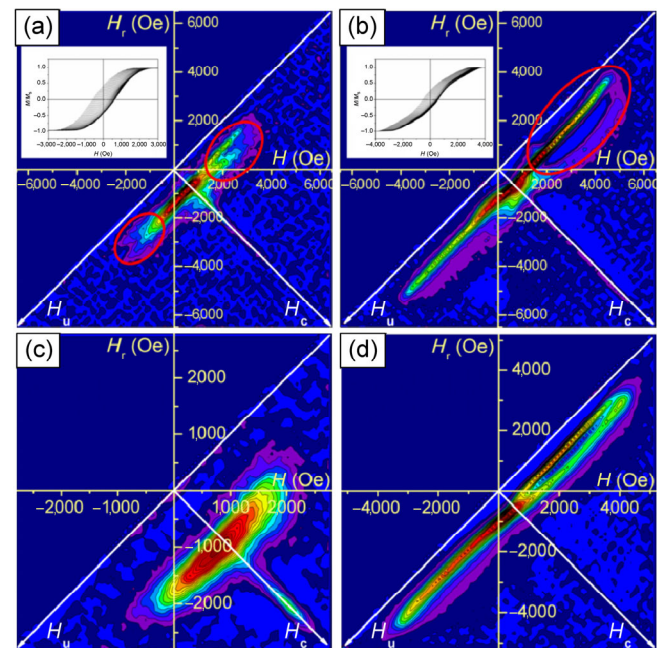

Figure 5 FORC distribution diagrams for the bi-segmented Ni nanowire arrays: (a) sample Ni-1 and (b) sample Ni-2. Insets in (a) and (b) show the FORC curves used for calculating the respective FORC diagrams. FORC diagrams for arrays of nanowires with homogeneous diameter: (c) sample Ni-4 and (d) sample Ni-5.

Table 3 Coercive field, H_c^{FORC}, and interaction field, ΔH_u, extracted from FORC diagrams of bi-segmented Ni nanowires (samples: Ni-1 and Ni-2) and with homogeneous diameter (samples: Ni-3, Ni-4 and Ni-5)

Sample	H_c^{FORC} (Oe)	ΔH_u (Oe)
Ni-1	710	920
Ni-2	740	770
Ni-3	670	490
Ni-4	920	870
Ni-5	550	700

Figure 4 Representative hysteresis loops of nanowire arrays measured by VSM under applied magnetic fields parallel (||) or perpendicular (⊥) to the nanowire axis, and the AFD curves calculated from perpendicular hysteresis loops for: (a) bi-segmented and (b) straight Ni nanowires; (c) bi-segmented and (d) straight FeCo nanowires.

nanowires into the array and the higher magnetic moment of the sample, but the uniaxial anisotropy and coercivity decrease as the diameter of the nanowires is increased, as a consequence of the different aspect ratios (length/diameter) of the samples [46].

For bi-segmented FeCo nanowire arrays (Figs. 6(a)–6(c)), a similar magnetic behavior to that of bi-segmented Ni nanowire arrays is observed, in the sense that the FORC distribution shows a broadening parallel to the interaction field axis around two different values of coercive field, being ascribed to the difference in diameter of the two segments [23, 27]. The interaction field value is much higher than for the Ni nanowires (Tables 3 and 4) indicating stronger demagnetizing interactions, which is ascribed to the much larger value of the saturation magnetization of FeCo alloy nanowires compared to Ni nanowires.

For FeCo nanowires with homogeneous diameter, the split coercivity distribution is not observed, presenting only one branch in their FORC diagrams (Figs. 6(d)–6(f)), with an increased interaction field (Table 4) as the nanowire diameter is larger (see that the interaction field for nanowires with 80 nm in diameter in Fig. 6(f) is larger than that for nanowires with 40 nm in diameter in Fig. 6(d)). On the other hand, for the nanowires with the smaller diameter, the FORC diagram shows the so-called wishbone shape (Fig. 6(d)), which presents a demagnetizing mean interaction field but with a non-negligible coercive field distribution. This type of

FORC distribution corresponds to a magnetic system with a strong reduction in the magnetostatic interactions between nanowires [47, 48], which can be explained by the reduction of the nanowire diameter and, consequently, the increase in the distance between neighbouring nanowires.

4   Conclusions

A combined fabrication process carried out through anodization, pore widening and atomic layer deposition was used to synthesize nanoporous alumina templates with hexagonally ordered pores having one well-defined geometrical modulation in the diameter along their length. Ni and $Fe_{50}Co_{50}$ nanowires were grown into the tailored-made alumina membranes by electroplating, in order to replicate the tuned geometry of the alumina templates with bi-segmented pores. All the nanowires showed a polycrystalline crystallographic structure being fcc with (220) preferential growing direction for Ni nanowires, and bcc structure along (110) preferential direction for FeCo nanowires.

An uniaxial easy magnetization axis was determined for all the bi-segmented diameter modulated nanowires, being the magnetization reversal process through the propagation of domain wall taking place by steps due to the geometrical modulation in diameter. This was observed in the shape of the hysteresis loops as they exhibit different values of magnetic susceptibilities when ranging the applied field, which results in two differentiated AFD peaks that correspond to each segment of the diameter modulated nanowires. The FORC diagrams show that the typical distribution for a nanowire array is partially transformed into a FORC diagram showing two split branches around two different values of coercive field which correlates to the difference in the segments diameter of bi-segmented nanowires, independently of their composition. The results reported in this work show that the FORC method as a powerful technique to determine the magnetic behavior of nanowire arrays, showing details of the magnetic behavior that are not possible to obtain by commonly used magnetometry techniques (i.e. measurement of major hysteresis loops).

The determination of the stepwise magnetization reversal process that takes place in the bi-segmented nanowires opens a promising

Table 4 Coercive field, H_c^{FORC}, and interaction field, ΔH_u, extracted from FORC diagrams of bi-segmented FeCo nanowires (samples: FeCo-1, FeCo-2 and FeCo-3) and with homogeneous diameter (samples: FeCo-4, FeCo-5, FeCo-6 and FeCo-7)

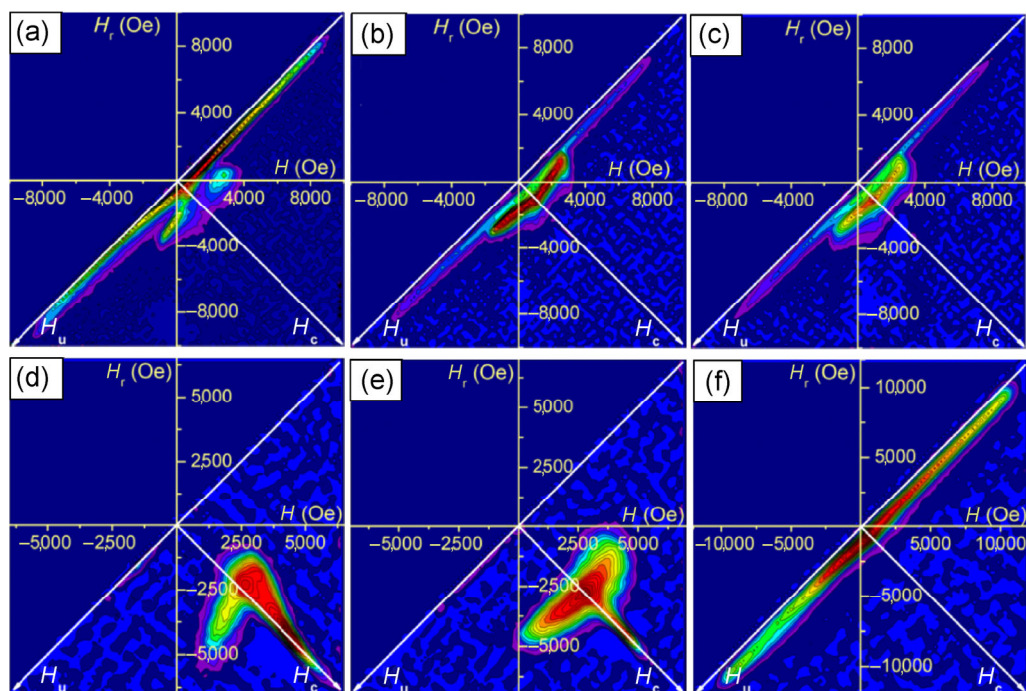| Sample	H_c^{FORC} (Oe)	ΔH_u (Oe)
FeCo-1	480	1,850
FeCo-2	980	2,070
FeCo-3	1,100	2,080
FeCo-4	2,810	720
FeCo-5	2,800	1,530
FeCo-6	530	3,530
FeCo-7	640	3,350

Figure 6 FORC diagrams for arrays of bi-segmented diameter modulated FeCo nanowires: (a) sample FeCo-1, (b) sample FeCo-2, and (c) sample FeCo-3; and for arrays of homogeneous diameter FeCo nanowires: (d) sample FeCo-4, (e) sample FeCo-5, and (f) sample FeCo-7.

path for the development of a new generation of information storage systems using this type of geometrically modulated nanowires, as the well-defined modulation in diameter will help to an advanced control of the remagnetization of nanowires.

In the bi-segmented ferromagnetic nanowires obtained by properly engineering a sharp and well-defined geometrical modulation in the nanowire diameter, each nanowire segment behaves with independent magnetization reversal process. The latter constitutes a fundamental key point for the development of novel ultrahigh-density data storage devices based on magnetic nanowire arrays with controlled reversal modes by tailored domain wall movement along nanowires, such as in racetrack memories.

Acknowledgements

Electronic Supplementary Material: Supplementary material (experimental details of electrochemical synthesis and characterization of nanowires, XRD patterns, and magnetic properties obtained from hysteresis loops) is available in the online version of this article at https://doi.org/10.1007/s12274-019-2385-9.

References

[1] Allwood, D. A.; Xiong, G; Faulkner, C. C.; Atkinson, D.; Petit, D.; Cowburn, R. P. Magnetic domain-wall logic. *Science* **2005**, *309*, 1688–1692.

[2] Allwood, D. A.; Xiong, G.; Cowburn, R. P. Writing and erasing data in magnetic domain wall logic systems. *J. Appl. Phys.* **2006**, *100*, 123908.

[3] Parkin, S. S. P.; Hayashi, M.; Thomas, L. Magnetic domain-wall racetrack memory. *Science* **2008**, *320*, 190–194.

[4] Hayashi, M.; Thomas, L.; Moriya, R.; Rettner, C.; Parkin, S. S. P. Current-controlled magnetic domain-wall nanowire shift register. *Science* **2008**, *320*, 209–211.

[5] Kou, X. M.; Fan, X.; Dumas, R. K.; Lu, Q.; Zhang, Y. P.; Zhu, H.; Zhang, X. K.; Liu, K.; Xiao, J. Q. Memory effect in magnetic nanowire arrays. *Adv. Mater.* **2011**, *23*, 1393–1397.

[6] Lee, D. J.; Kim, E.; Kim, D.; Park, J.; Hong, S. Nano-storage wires. *ACS Nano* **2013**, *7*, 6906–6913.

[7] Grutter, A. J.; Krycka, K. L.; Tartakovskaya, E. V.; Borchers, J. A.; Reddy, K. S. M.; Ortega, E.; Ponce, A.; Stadler, B. J. H. Complex three-dimensional magnetic ordering in segmented nanowire arrays. *ACS Nano* **2017**, *11*, 8311–8319.

[8] Sergelius, P.; Moreno, J. M. M.; Rahimi, W.; Waleczek, M.; Zierold, R.; Görlitz, D.; Nielsch, K. Electrochemical synthesis of highly ordered nanowires with a rectangular cross section using an in-plane nanochannel array. *Nanotechnology* **2014**, *25*, 504002.

[9] Pitzschel, K.; Moreno, J. M. M.; Escrig, J.; Albrecht, O.; Nielsch, K.; Bachmann, J. Controlled introduction of diameter modulations in arrayed magnetic iron oxide nanotubes. *ACS Nano* **2009**, *3*, 3463–3468.

[10] Esmaeily, A. S.; Venkatesan, M.; Razavian, A. S.; Coey, J. M. D. Diameter-modulated ferromagnetic CoFe nanowires. *J. Appl. Phys.* **2013**, *113*, 17A327.

[11] Minguez-Bacho, I.; Rodriguez-López, S.; Vázquez, M.; Hernández-Vélez, M.; Nielsch, K. Electrochemical synthesis and magnetic characterization of periodically modulated Co nanowires. *Nanotechnology* **2014**, *25*, 145301.

[12] Prida, V. M.; García, J.; Iglesias, L.; Vega, V.; Görlitz, D.; Nielsch, K.; Barriga-Castro, E. D.; Mendoza-Reséndez, R.; Ponce, A.; Luna, C. Electroplating and magnetostructural characterization of multisegmented $Co_{54}Ni_{46}/Co_{85}Ni_{15}$ nanowires from single electrochemical bath in anodic alumina templates. *Nanoscale Res. Lett.* **2013**, *8*, 263.

[13] Méndez, M.; González, S.; Vega, V.; Teixeira, J. M.; Hernando, B.; Luna, C.; Prida, V. M. Ni-Co alloy and multisegmented Ni/Co nanowire arrays modulated in composition: Structural characterization and magnetic properties. *Crystals* **2017**, *7*, 66.

[14] Salem, M. S.; Tejo, F.; Zierold, R.; Sergelius, P.; Moreno, J. M. M.; Goerlitz, D.; Nielsch, K.; Escrig, J. Composition and diameter modulation of magnetic nanowire arrays fabricated by a novel approach. *Nanotechnology* **2018**, *29*, 065602.

[15] Neumann, R. F.; Bahiana, M.; Allende, S.; Altbir, D.; Görlitz, D.; Nielsch, K. Tailoring the nucleation of domain walls along multi-segmented cylindrical nanoelements. *Nanotechnology* **2015**, *26*, 215701.

[16] Méndez, M.; Vega, V.; González, S.; Caballero-Flores, R.; García, J.; Prida, V. M. Effect of sharp diameter geometrical modulation on the magnetization reversal of bi-segmented FeNi nanowires. *Nanomaterials* **2018**, *8*, 595.

[17] Bochmann, S.; Döhler, D.; Trapp, B.; Staňo M.; Fruchart, O.; Bachmann J. Preparation and physical properties of soft magnetic nickel-cobalt three-segmented nanowires. *J. Appl. Phys.* **2018**, *124*, 163907.

[18] Pitzschel, K.; Bachmann, J.; Martens, S.; Montero-Moreno, J. M.; Kimling, J.; Meier, G.; Escrig, J.; Nielsch, K.; Görlitz, D. Magnetic reversal of cylindrical nickel nanowires with modulated diameters. *J. Appl. Phys.* **2011**, *109*, 033907.

[19] Burn, D. M.; Arac, E.; Atkinson, D. Magnetization switching and domain-wall propagation behavior in edge-modulated ferromagnetic nanowire structures. *Phys. Rev. B* **2013**, *88*, 104422.

[20] Salem, M. S.; Sergelius, P.; Corona, R. M.; Escrig, J.; Görlitz D.; Nielsch, K. Magnetic properties of cylindrical diameter modulated $Ni_{80}Fe_{20}$ nanowires: Interaction and coercive fields. *Nanoscale* **2013**, *5*, 3941–3947.

[21] Zeng, H.; Michalski, S.; Kirby, R. D.; Sellmeyer, D. J.; Menon, L.; Bandyopadhyay, S. Effects of surface morphology on magnetic properties of Ni nanowire arrays in self-ordered porous alumina. *J. Phys. Condens. Mat.* **2002**, *14*, 715–721.

[22] Kumar, A.; Fähler, S.; Schlörb, H.; Leistner, K.; Schultz, L. Competition between shape anisotropy and magnetoelastic anisotropy in Ni nanowires electrodeposited within alumina templates. *Phys. Rev. B* **2006**, *73*, 064421.

[23] Bran, C.; Palmero, E. M.; Li, Z. A.; del Real, R. P.; Spasova, M.; Farle, M.; Vázquez, M. Correlation between structure and magnetic properties in Co_xFe_{100-x} nanowires: The roles of composition and wire diameter. *J. Phys. D: Appl. Phys.* **2015**, *48*, 145304.

[24] Palmero, E. M.; Bran, C.; del Real, R. P.; Vázquez, M. Vortex domain wall propagation in periodically modulated diameter FeCoCu nanowire as determined by the magneto-optical Kerr effect. *Nanotechnology* **2015**, *26*, 461001.

[25] Bran, C.; Berganza, E.; Palmero, E. M.; Fernandez-Roldan, J. A.; del Real, R. P.; Aballe, L.; Foerster, M.; Asenjo, A.; Fraile Rodriguez, A.; Vazquez, M. Spin configuration of cylindrical bamboo-like magnetic nanowires. *J. Mater. Chem. C* **2016**, *4*, 978–984.

[26] Hertel, R.; Kirschner, J. Magnetization reversal dynamics in nickel nanowires. *Phys B: Condens. Matter* **2004**, *343*, 206–210.

[27] Ivanov, Y. P.; Vázquez, M.; Chubykalo-Fesenko, O. Magnetic reversal modes in cylindrical nanowires. *J. Phys. D: Appl. Phys.* **2013**, *46*, 485001.

[28] Bran, C.; Ivanov, Y. P.; García, J.; del Real, R. P.; Prida, V. M.; Chubykalo-Fesenko, O.; Vazquez, M. Tuning the magnetization reversal process of FeCoCu nanowire arrays by thermal annealing. *J. Appl. Phys.* **2013**, *114*, 043908.

[29] Vock, S.; Hengst, C.; Wolf, M.; Tschulik, K.; Uhlemann, M.; Sasvári, Z.; Makarov, D.; Schmidt, O. G.; Schultz, L.; Neu, V. Magnetic vortex observation in FeCo nanowires by quantitative magnetic force microscopy. *Appl. Phys. Lett.* **2014**, *105*, 172409.

[30] Spinu, L.; Stancu, A.; Radu, C.; Li, F.; Wiley, J. B. Method for magnetic characterization of nanowire structures. *IEEE Trans. Magn.* **2004**, *40*, 2116–2118.

[31] Béron, F.; Clime, L.; Ciureanu, M.; Ménard, D.; Cochrane, R. W.; Yelon, A. Magnetostatic interactions and coercivities of ferromagnetic soft nanowires in uniform length arrays. *J. Nanosci. Nanotechnol.* **2008**, *8*, 2944–2954.

[32] Navas, D.; Torrejon, J.; Béron, F.; Redondo, C.; Batallan, F.; Toperverg, B. P.; Devishvili, A.; Sierra, B.; Castaño, F.; Pirota, K. R. et al. Magnetization reversal and exchange bias effects in hard/soft ferromagnetic bilayers with orthogonal anisotropies. *New J. Phys.* **2012**, *14*, 113001.

[33] Proenca, M. P.; Merazzo, K. J.; Vivas, L. G.; Leitao, D. C.; Sousa, C. T.; Ventura, J.; Araujo, J. P.; Vazquez, M. Co nanostructures in ordered templates: Comparative FORC analysis. *Nanotechnology* **2013**, *24*, 475703.

[34] Almasi-Kashi, M.; Ramazani, A.; Golafshan, E.; Arefpour, M.; Jafari-Khamse, E. First order reversal curve investigation of the hard and soft magnetic phases of annealed CoFeCu nanowire arrays. *Phys B: Condens. Matter* **2013**, *429*, 46–51.

[35] Palmero, E. M.; Béron, F.; Bran, C.; del Real, R. P.; Vázquez, M. Magnetic interactions in compositionally modulated nanowire arrays. *Nanotechnology* **2016**, *27*, 435705.

[36] Béron, F.; Pirota, K. R.; Vega, V.; Prida, V. M.; Fernández, A.; Hernando, B.; Knobel, M. An effective method to probe local magnetostatic properties in a nanometric FePd antidot array. *New J. Phys.* **2011**, *13*, 013035.

[37] Bachmann, J.; Zierold, R.; Chong, Y. T.; Hauert, R.; Sturm, C.; Schmidt-Grund, R.; Rheinländer, B.; Grundmann, M.; Gösele, U.; Nielsch, K. A practical, self-catalytic, atomic layer deposition of silicon dioxide. *Angew. Chem., Int. Ed.* **2008**, *47*, 6177–6179.

[38] Dobrotă, C. I.; Stancu, A. What does a first-order reversal curve diagram really mean? A study case: Array of ferromagnetic nanowires. *J. Appl. Phys.* **2013**, *113*, 043928.

[39] Barandiaran, J. M.; Vázquez, M.; Hernando, A.; González, J.; Rivero, G. Distribution of the magnetic anisotropy in amorphous alloys ribbons. *IEEE Trans. Magn.* **1989**, *25*, 3330–3332.

[40] Vega, V.; Böhnert, T.; Martens, S.; Waleczek, M.; Montero-Moreno, J. M.; Görlitz, D.; Prida, V. M.; Nielsch, K. Tuning the magnetic anisotropy of Co–Ni nanowires: Comparison between single nanowires and nanowire arrays in hard-anodic aluminum oxide membranes. *Nanotechnology* **2012**, *23*, 465709.

[41] Béron, F.; Ménard, D.; Yelon, A. First-order reversal curve diagrams of magnetic entities with mean interaction field: A physical analysis perspective. *J. Appl. Phys.* **2008**, *103*, 07D908.

[42] Béron, F.; Carignan, L. P.; Ménard, D.; Yelon, A. Extracting individual properties from global behaviour: First-order reversal curve method applied to magnetic nanowire arrays. In *Electrodeposited Nanowires and Their Applications*; Lupu, N., Ed.; IntechOpen: Vienna, 2010; pp 167–188.

[43] Rotaru, A.; Lim, J. H.; Lenormand, D.; Diaconu, A.; Wiley, J. B.; Postolache, P.; Stancu, A.; Spinu, L. Interactions and reversal-field memory in complex magnetic nanowire arrays. *Phys. Rev. B* **2011**, *84*, 134431.

[44] Samanifar, S.; Almasi Kashi, M.; Ramazani, A.; Alikhani, M. Reversal modes in FeCoNi nanowire arrays: Correlation between magnetostatic interactions and nanowires length. *J. Magn. Magn. Mater.* **2015**, *378*, 73–83.

[45] Sergelius, P.; Fernandez, J. G.; Martens, S.; Zocher, M.; Böhnert, T.; Martinez, V. V.; de la Prida, V. M.; Görlitz, D.; Nielsch, K. Statistical magnetometry on isolated NiCo nanowires and nanowire arrays: A comparative study. *J. Phys. D: Appl. Phys.* **2016**, *49*, 145005.

[46] Raposo, V.; Zazo, M.; Flores, A. G.; García, J.; Vega, V.; Iñiguez, J.; Prida, V. M. Ferromagnetic resonance in low interacting permalloy nanowire arrays. *J. Appl. Phys.* **2016**, *119*, 143903.

[47] Pike, C. R.; Ross, C. A.; Scalettar R. T.; Zimanyi, G. First-order reversal curve diagram analysis of a perpendicular nickel nanopillar array. *Phys. Rev. B* **2005**, *71*, 134407.

[48] García, J.; Vega, V.; Thomas, A.; Prida, V. M.; Nielsch, K. Two-step magnetization reversal FORC fingerprint of coupled bi-segmented Ni/Co magnetic nanowire arrays. *Nanomaterials* **2018**, *8*, 548.